Laser speckle contrast imaging of cerebral blood flow in humans during neurosurgery: a pilot clinical study

Ashwin B. Parthasarathy
Erica L. Weber
Lisa M. Richards
The University of Texas at Austin
Department of Biomedical Engineering
Austin, Texas 78712

Douglas J. Fox
St. David's Hospital
NeuroTexas Institute
Austin, Texas 78705

Andrew K. Dunn
The University of Texas at Austin
Department of Biomedical Engineering
Austin, Texas 78712

Abstract. Monitoring cerebral blood flow (CBF) during neurosurgery can provide important physiological information for a variety of surgical procedures. CBF measurements are important for assessing whether blood flow has returned to presurgical baseline levels and for assessing postsurgical tissue viability. Existing techniques for intraoperative monitoring of CBF based on magnetic resonance imaging are expensive and often impractical, while techniques such as indocyanine green angiography cannot produce quantitative measures of blood flow. Laser speckle contrast imaging (LSCI) is an optical technique that has been widely used to quantitatively image relative CBF in animal models *in vivo*. In a pilot clinical study, we adapted an existing neurosurgical operating microscope to obtain LSCI images in humans in real time during neurosurgery under baseline conditions and after bipolar cautery. Simultaneously recorded ECG waveforms from the patient were used to develop a filter that helped reduce measurement variabilities due to motion artifacts. Results from this study demonstrate the feasibility of using LSCI to obtain blood flow images during neurosurgeries and its capability to produce full field CBF image maps with excellent spatial resolution in real-time with minimal disruption to the surgical procedure. © *2010 Society of Photo-Optical Instrumentation Engineers.* [DOI: 10.1117/1.3526368]

Keywords: laser speckle contrast imaging; intraoperative imaging; flow measurement; scattering spectroscopy; cerebral blood flow.

Paper A10394R received Jul. 12, 2010; revised manuscript received Oct. 26, 2010; accepted for publication Nov. 5, 2010; published online Dec. 30, 2010.

1 Introduction

Monitoring cerebral blood flow (CBF) during surgery is important during a variety of surgical procedures. In procedures such as clipping of aneurysms or vessel bypass, CBF measurements can help assess if blood flow has returned to presurgical baseline levels. In other procedures such as tumor resections, CBF measurements can help assess postsurgical tissue viability. CBF measures can also be used to identify motor, sensory, and speech activation centers in the cortex in procedures that require functional localization. Although the importance of imaging CBF during surgery is well known, there are not many techniques that can produce real-time CBF images with minimum interference to the surgery. For this reason, *in vivo* measurements of blood flow during surgeries have been underutilized as a surgical tool.

Most traditional blood flow measurement techniques are impractical for intraoperative imaging because they are usually intrusive. Intraoperative flow measurement techniques based on magnetic resonance imaging are difficult to use because they need special operating room conditions.[1] Optical imaging techniques provide a unique window into brain function using various intrinsic and extrinsic contrast agents.[2] Researchers have used optical imaging of intrinsic signals to visualize language[3] and epilepsy centers[4] intraoperatively during human

brain surgery. The most promising flow measurement technique that is currently being used for imaging CBF is indocyanine green (ICG)-based angiography.[5,6] ICG angiography involves injecting a dye (ICG) into the blood stream, exciting it with an infrared light source, and imaging the fluorescence intensity with a camera. Commercial systems have managed to integrate ICG measurements into existing microscope systems. But because the contrast mechanism for imaging blood flow is fluorescence intensity, these measurements can, at best, detect the presence or absence of blood flow in a vessel and hence are not quantitative. Lack of quantitative measures and the need to repeatedly inject a dye to make measurements are the major limitations of ICG-based angiography. Hence, there is a need to develop a technique to image CBF during surgery, that: (a) is minimally intrusive to the surgical procedure, (b) can produce quantitative measures of changes in blood flow, and (c) has real-time capabilities.

Optical flow measurement techniques that are based on dynamic light scattering have the potential to satisfy these requirements. Laser Doppler techniques can provide quantitative flow information but are traditionally restricted to single point measurements with probes that are cumbersome to handle and not repeatable. Recently, Raabe et al. demonstrated CBF measurements intraoperatively using a full-field laser Doppler instrument[7] at low temporal resolutions. Laser speckle contrast imaging (LSCI) is an optical imaging technique that has great

Address all correspondence to: Andrew K. Dunn, The University of Texas at Austin, Department of Biomedical Engineering, Austin, Texas 78712; Tel: 512-232-2808; E-mail: adunn@mail.utexas.edu

potential to obtain minimally intrusive, quantitative measures of blood flow with good spatial resolution in real time. Briefly, in LSCI photons from a coherent light source travel slightly different path lengths in tissue to create a random interference pattern on a detector called speckle. When these photons scatter off moving particles, such as red blood cells in cortical vessels, they undergo a phase shift that causes temporal fluctuations in the speckle pattern. The speed of the blood flow within the vessels is related to the time scale of these temporal fluctuations and are hence estimated by quantifying the localized spatial variance of the speckle pattern. Several recent review papers have described the basic theory and instrumentation of LSCI and its use in a wide variety of applications.[8,9]

LSCI has been used to study a wide variety of physiological phenomena,[10–17] such as ischemic stroke, cortical spreading depressions, and functional activation in animals. Similar to their applications in research studies, clinical measurements of blood flow can provide vital information about tissue perfusion and viability (for diagnosis)[18] and vessel functionality (during surgery). Recently, Hecht et al. demonstrated LSCI's use in measuring CBF during surgery with a commercial laser speckle instrument.[19] Although this was the first intraoperative application of LSCI, the use of a commercial instrument had its disadvantages. Primarily, the instrument was not integrated with the surgical procedure and hence needed additional setup time, making the measurements intrusive toward the surgery. Additionally, the blood flow measures in this study were quantified in arbitrary units of flux and the speed of image acquisition and processing is low. In this paper, we present results from a pilot clinical study $(n = 3)$, where LSCI was used to image CBF in humans during neurosurgeries in a minimally intrusive way, by adapting an existing neurosurgical microscope. Our system has the capability to produce full field $(\sim650 \times 500$ pixels) blood flow maps at rates of 100 fps. Blood flow measurements in the human brain can be especially challenging because, during neurosurgery, the brain is no longer contained by the skull and hence has a tendency to be pulsatile. To remove measurement variability due to this motion artifact, we developed and applied a filter using simultaneously recorded ECG waveforms from each patient.

2 Instrumentation

LSCI automatically lends itself to address two of the three desired characteristics for measuring CBF during surgeries. LSCI's ability to measure flow changes quantitatively has been well documented.[10,11] LSCI's biggest strength is in the use of simple instrumentation to image blood flow. The standard LSCI instrument requires illuminating the sample with a coherent light source and imaging the backscattered light using a camera. This simple instrumentation and low cost make LSCI an attractive technology for imaging CBF during neurosurgery. Additionally, because these measurements can be made with fast cameras, they offer excellent temporal resolution. By incorporating new processing techniques[20] in our custom-written data-acquisition software, we can obtain, compute, and display real-time measures of CBF. These improvements allow our intraoperative LSCI instrument to display full-field CBF images at ~70–100 Hz, a temporal resolution

that is ~50 times greater than previous intraoperative LSCI measurements.[19]

The primary design consideration for an LSCI instrument that would be used as a neurosurgical tool was to adapt the technique in a way that it offers minimum interference to the surgical procedure. To achieve this, an existing Zeiss OPMI neurosurgical operating microscope (Carl Zeiss Meditec Inc., Dublin, California) was retrofitted with a camera and a single-mode diode laser to obtain speckle images as shown in Fig. 1(a). Figure 1(b) shows a schematic that illustrates the functioning of the intraoperative LSCI instrument. A camera (Basler 602f, Basler Vison Technologies, Germany) was connected through a camera adapter to one of the existing viewing ports of the microscope. This enabled the use of optics and mechanics present in the microscope to produce and focus the image on the camera. As an added advantage, because existing microscope controls were used, the surgeons who were familiar with the functioning of the microscope found it easy to operate the adapted LSCI instrument. This advantage is a significant improvement over previous efforts to image CBF intraoperatively, making it minimally invasive to the surgery and eliminating the need to train surgeons to operate a new instrument. To illuminate the brain, a laser diode $(\lambda = 660$ nm, $P = 90$ mW) was connected to a microscope add-on laser adapter and attached to the neurosurgical microscope. The adapter delivered laser light through a pair of relay lenses to a mirror mounted on the inside of the microscope aperture. The mirror has steering mechanisms in place to direct the laser beam over the field of view of the camera. The illumination path is illustrated in the schematic in Fig. 1(b). The surgical microscope's illumination was tured off during the imaging sessions. The average laser power incident on the brain was measured to be ≈28 mW/cm^2. This is less than the average incident power due to the inbuilt illumination from the surgical microscope $(\approx30$ mW/cm$^2)$ and well within the ANSI standard of 200 mW/cm^2.[21]

The addition of the camera and laser did not interfere with the normal sterile draping of the microscope. Additionally, the patient's electrocardiogram (ECG) was recorded by the computer as a reference point for the measurements. The ECG waveforms were obtained from existing anesthesia monitoring systems present in the operating room. The ECG measurements were time synchronized with image aquisition. It was used to develop an *ad hoc* filter, designed to filter out the effect of pulsatile motion in the brain. Because additional equipment was not brought in to perform CBF imaging, the time taken for these measurements is reduced significantly and the surgical procedure is not interrupted. This is a significant advantage of this system over previous attempts.[19]

3 Experimental Methods

The primary focus of the pilot clinical study $(n = 3)$ was to use the modified surgical microscope to image cerebral vasculature during neurosurgery and demonstrate the feasibility of using LSCI in a minimally obtrusive way to obtain intraoperative CBF measures and to characterize baseline fluctuations in speckle contrast due to pulsation of the exposed brain. All experiments were performed during tumor resection surgeries performed at the NeuroTexas Institute in St. Davids Hospital in Austin, Texas.
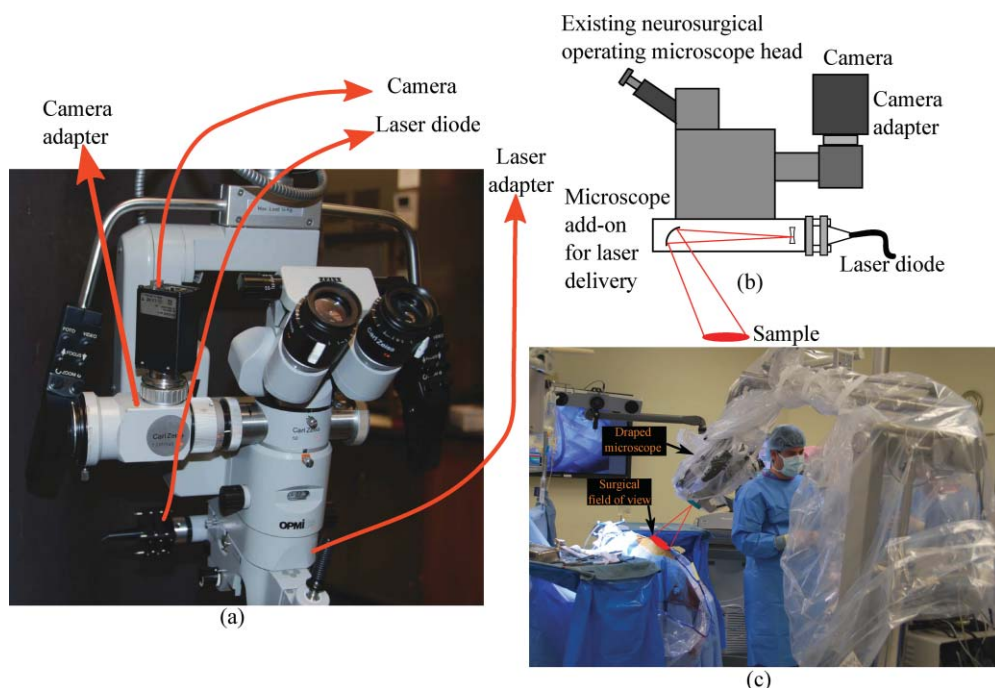
Fig. 1 Zeiss OPMI microscope adapted to measure CBF using LSCI. (a) A camera is attached to an existing viewing port in the microscope and a diode laser is attached to an add-on laser adapter. The microscope's existing controls make it easy for the surgeon to position and focus it. (b) Schematic of the instrumentation. The laser adapter delivers light which is colocated with the microscope's light source. (c) The adapted microscope in use during an imaging session. The microscope has been covered in a sterile drape. The surgeon is seen viewing the images on a remote monitor after positioning the microscope over the field of view.

The pilot clinical study was approved by the Institutional Review Boards of the University of Texas at Austin and St. David's Hospital.

Before each surgery, the microscope was set up, initialized, and then draped using a standard surgical microscope drape, as shown in Fig. 1(c). After the surgeon completed the craniotomy over the surgical area, the microscope was positioned and images were obtained for ∼15 min at a rate of 100 Hz with an exposure duration of 5 ms. At 5 ms exposure duration, the ambient surgical room lights do not affect imaging and hence they do not have to be turned off. Before each imaging session, the surgical area was flushed with physiologically sterile warmed saline to reduce specular reflections. The ECG waveform was recorded along with the camera exposure signals for filtering as described below. The ECG filtering for all data sets was performed after data acquisition. Table 1 lists the experimental procedures, their specific case, and imaging details.

4 Results

Raw speckle images obtained in the experiments were converted to speckle contrast images using

$$K = \frac{\sigma_s}{\langle I \rangle}, \qquad (1)$$

where σ_s and $\langle I \rangle$ are the standard deviation and mean of intensities in a 7×7 pixel region of the image. The speckle contrast image was created by moving this window over the raw speckle image. More details on computing the speckle contrast from raw speckle images can be found in literature.[10]

The speckle contrast images were converted into a more quantitative measure of blood flow, correlation time τ_c, using

$$K(T, \tau_c) = \beta \frac{e^{-2(T/\tau_c)} - 1 + 2(T/\tau_c)}{2(T/\tau_c)^2}^{1/2}, \qquad (2)$$

where T is the exposure duration of the camera, β is an instrumentation factor and τ_c is the correlation time, a measure of blood flow. The correlation time, τ_c, is the average decay time of speckle electric field autocorrelation function. τ_c is a more quantitative measure of blood flow than speckle contrast K or other arbitrary units of CBF. The validity of using τ_c as a measure of CBF has previously been verified by many researchers.[10,13,22] The instrumentation factor β depends primarily on the number of speckles imaged onto a single camera pixel[23,24] as well as a number of other factors, such as the polarization of light.[25] Because the exact value of β is difficult to estimate,[24,26] β was assumed to be equal to 1 for computing the correlation time τ_c. Although this assumption is not entirely accurate, an inaccurate estimate of β only affects the absolute value of correlation time and estimates of relative changes in correlation time (and hence blood flow) are not affected by this assumption.

The speckle contrast image obtained by imaging the cerebral cortex of the first patient is shown in Fig. 2(a). These images were obtained before the tumor was resected and are primarily surface vasculature. Despite flushing the surgical field of view with saline, some spots of specular reflection are visible. Specular reflection causes some camera pixels to saturate and hence manifest themselves as dark spots in the speckle contrast image. Figure 2(b) shows the spatial correlation time map (displayed on a logarithmic scale) computed using Eq. (2) as described earlier.

Table 1 List of experiments. The imaging sessions were on tumor recession surgeries. Imaging of the cortex was done before the tumor was resected in the first patient and after the tumor was resected in the second and third patients. The flexibility of the instrumentation can be seen in its ability to image the cortex in a variety of different cortical regions.

Patient No.	Surgery	Surgery Details	Imaging Details
1, M, 52 years old	Tumor resection	Right temporal lobe (just under the surface)	Imaged before tumor recession
2, M, 33 years old	Tumor resection	Right hemisphere	Imaged after tumor recession
3, F, 57 years old	Tumor resection	Left temporal meningioma	Imaged after tumor recession

Vessels of different sizes and flow rates can be clearly visualized in both the speckle contrast and correlation time maps.

Figure 3 shows the speckle contrast and correlation time maps obtained from the cerebral cortex of patient 2. Although vasculature is still clearly visible, the quality of the image is not as good as in Fig. 2(a). The primary reason for this is that these images were obtained after the tumor was removed. Consequently, these images are not from surface vasculature but rather from deeper cortical regions, exposed by the resection of brain tissue during surgery. Additionally, this specific patient had previous history of brain surgery, which coupled with the current surgery caused bruising in the brain. Because deeper cortical regions were imaged, imaging was performed at a steep angle, utilizing the flexibility of the microscope [Fig. 1(c)]. Figure 3(b) shows the correlation time map computed using Eq. (2). Vasculature and blood flow are spatially resolved in both the speckle contrast and correlation time spatial maps.

In one subject (patient 3), we observed a significant change in blood flow when imaging during the process of surgical hemostasis. Bipolar cautery was used during surgery in the top right-hand portion of the imaged area, represented by a blue oval in Fig. 4(a). Four regions [Fig. 4(a)] were identified in the field of view and the relative change in blood flow was computed for each region [shown in Fig. 4(b)]. First, the average correlation time in the regions was computed for all time points using the methods described above. An *ad hoc* ECG filter, described in more detail later, was applied to the data points and the filtered data were normalized to a baseline. The average correlation time in each region for the first 5 s was used a baseline for the measurements. We found that the cauterization procedure resulted in a reduction in blood flow in all regions followed by a transient increase in blood flow. The increase in blood flow a few minutes after the cauterization could be the result of a neuro-protective mechanism that prevents tissue damage due to loss of blood flow. These measurements illustrate the ability of the intraoperative LSCI instrument to measure blood flow changes at good spatial and temporal resolutions.

5 Discussion

One of the challenges in clinical measurement of CBF is the presence of artifacts, due to the pulsatile motion of the brain. These artifacts are primarily induced by the patient's breathing and heart beat as well as high intracranial pressures. The motion of the brain is not significant when the skull is intact. However, in a neurosurgical procedure, the exposed brain has a tendency to throb. Figure 5(b) shows the time course of measured correlation times (τ_c) from a region over a large vessel [region 1 in
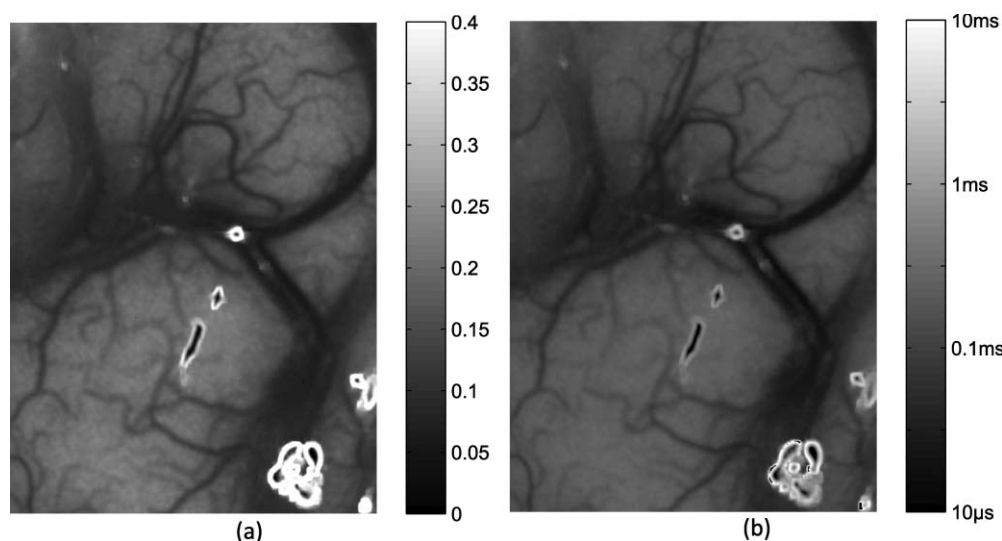

Fig. 2 Average of 30 LSCI images obtained using the adapted neurosurgical microscope from the cortex of a 52 year old male patient before tumor resection. Field of view of the image is ~2×1 cm. (a) Speckle contrast image showing cerebral vasculature. Regions with higher flow are represented by lower speckle contrast values. (b) Correlation time map (visualized on a logarithmic scale). The dark spots on the images correspond to specular reflection from the cortex.
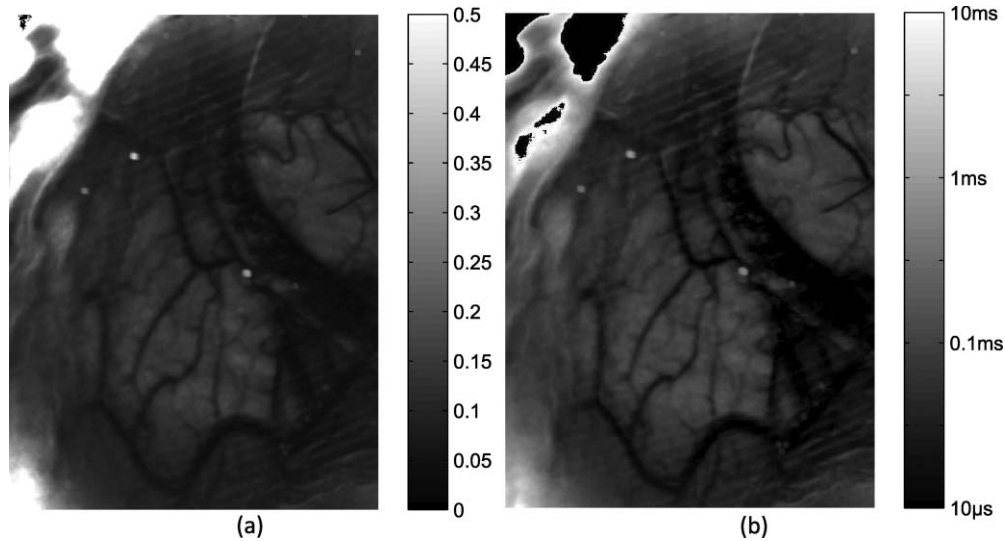
Fig. 3 Average of 30 LSCI images obtained using the adapted neurosurgical microscope from the cortex of a 33-year-old male patient after tumor resection. Field of view of the image is ∼ 2×1 cm. (a) Speckle contrast image showing cerebral vasculature. Regions with higher flow are represented by lower speckle contrast values. (b) Correlation time map (visualized on a logarithmic scale). The field of view that was imaged in this experiment was fairly deep in the cortex. The side of the cortex as visible in the top right corner of the image is characterized by an absence of vasculature.

Fig. 5(a)] from cortical imaging of patient 1. This time course is superimposed and synchronized in time with the ECG signals recorded from patient 1. From Fig. 5(b), the motion artifact due to pulsations of the brain can be observed. It is also observed that these pulsations are synchronized in time with the heart beats. It should be noted that we were able to resolve these fluctuations in CBF because of our increased temporal resolution of blood flow measures.

These pulsatile blood flow measures can be tolerated for basic visual inspection of CBF and would not hinder applications such as imaging blood flow during aneurysm surgeries and vessel bypass procedures. Also, these artifacts would not affect the ability of the instrument to detect large blood flow changes. However, applications such as functional activation are typically associated with a ∼ 5 to 10% change in blood flow.[7] In such cases, these fluctuations in correlation time measures would limit the signal to noise of estimating blood flow changes. Hence, there is a need to eliminate these fluctuations.

Because these fluctuations in the blood flow are synchronized and collocated with the heart beat, an *ad hoc* ECG detrending filter was designed to filter out these fluctuations. This filter is similar to an adaptive filter technique used for MRI time series data designed by Deckers et al.[27] The filter was designed based on the time of a camera exposure relative to the ECG cycle. The camera exposure signals and the ECG waveform were recorded during the imaging session. These waveforms were used to determine the actual times at which each speckle image was obtained, and the actual times of each heart beat. A
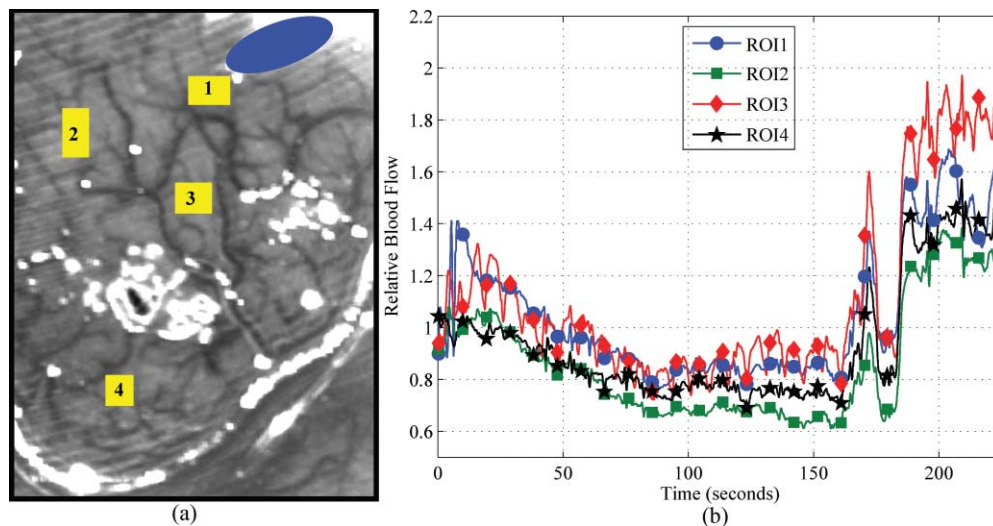

Fig. 4 (a) Speckle contrast image from cortical imaging of patient 3 describing position of bipolar cautery (blue oval) and regions of interest and (b) Relative blood flow changes in four regions of interest. τ_c measures from the first 5 s was used as the baseline. Relative blood flow measures show a gradual decrease in blood flow after cautery. This decrease in blood flow is followed by a transient increase.
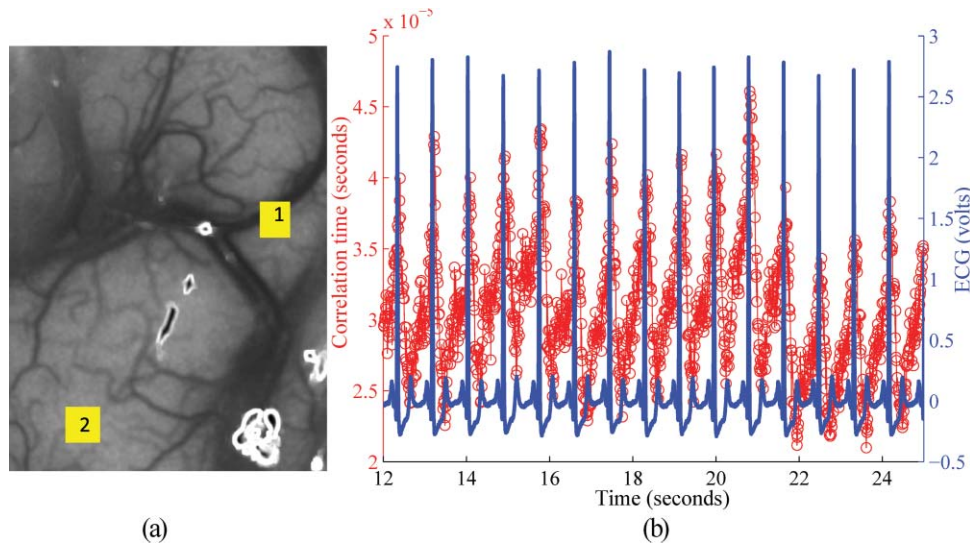
Fig. 5 (a) Speckle contrast image (5-ms exposure duration) obtained from patient 1. (b) Average correlation time measure in spatial region 1, synchronized with ECG recorded from patient 1. The pulsatile nature of blood flow is seen in the τ_c time course. The fluctuations are found to be synchronized with the heart beat.

filter function was generated from these times, which was the correlation time value as a function of "normalized time." The normalized time was defined as the time of image acquisition relative to the nearest heart beat. For example, if the camera was found to have exposed at a time t_{frame} seconds, and the nearest previous heart beat (of width t_{RR} seconds) was recorded at time t_{beat} seconds, then the normalized time for this frame would be

$$t_{\text{normalized}} = \frac{t_{\text{frame}} - t_{\text{beat}}}{t_{\text{RR}}}. \qquad (3)$$

Figure 6 illustrates this filter function generated from the first 20 s of data. The blue circles are the experimentally measured τ_c values within a region of interest plotted as a function of
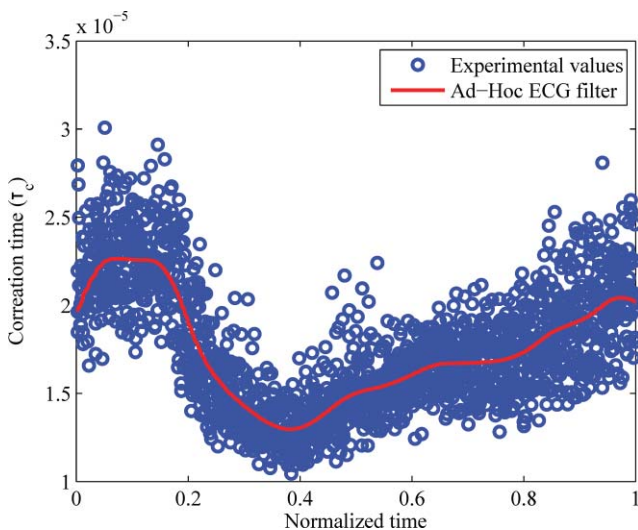

Fig. 6 *Ad hoc* ECG detrending filter designed from experimental values.

time within the cardiac cycle, while the red line is the filter function generated by averaging the experimental values using a moving average filter. Each value of the filter function represents the average ("artificial") rise or fall in correlation time at a specific time in the ECG cycle. Finally, the filter was applied to the data by estimating the normalized time of each data point, subtracting the corresponding filter value, and adding back the median correlation time value.

Figure 7 shows the time course over a 13 s duration (to illustrate filtering) of correlation time τ_c measured from cortical blood flow imaging of patient 1. Figure 7(a) is the time course from region 1 [Fig. 5(a)]—a large vessel, whereas Fig. 7(b) is the time course from region 2 [Fig. 5(a)]—the parenchyma. Two observations can be made from the unfiltered time-course measurements: (i) the correlation time measures in the parenchyma is approximately one order of magnitude higher than those measured from the vessel, which is around expected lines, and (ii) fluctuations are present in measurements from both regions, which indicates that the motion artifact is present throughout the field of view. The red curve in both cases represents the result of applying the *ad hoc* ECG filter on the experimental measurements. The noise in the filtered measurements was reduced by using a moving average filter of width 0.05 s. This filtered curve is represented by the black curve. For the unfiltered and filtered data sets, the variation in correlation time over the span of one heart beat was estimated by computing normalized standard deviation of τ_c values. The variation of τ_c averaged over 14 heart beats is listed in Table 2.

Visual inspection (Fig. 7) and quantitative comparison (Table 2) both confirm that the filtering techniques we use effectively reduce the variation in correlation times during a heart beat. Unsurprisingly, the moving average filter with a width of 0.5 s, being a low pass filter, produces the most significant reduction in variance of τ_c (Table 2). However, the moving average filter reduces the variability in τ_c due to the motion artifact as well as the inherent variability in τ_c due to physiology. The *ad hoc* filter retains this inherent physiological variablity while
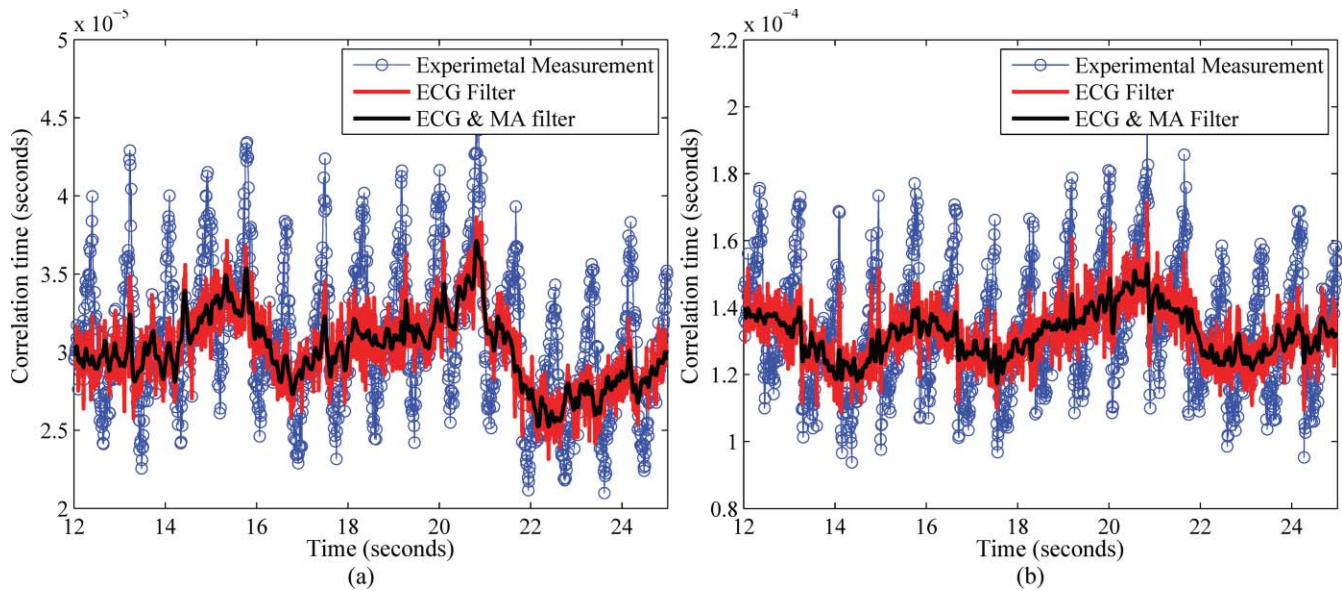
Fig. 7 Time course of correlation time (τ_c) from (a) region 1 and (b) region 2; obtained from patient 1 [Fig. 5(a)]. The red trace in both time courses represent the result of correlation time course filtered to remove motion artifact due to pulsatile brain motion. The black line in both time courses is a moving average filter applied to the result of the *ad hoc* ECG filter. The rise and fall of τ_c due to the heart beat is removed by filtering, while changes in the baseline τ_c values are retained.

removing τ_c variations due to the motion artifact alone. By combining the *ad hoc* ECG filter and a moving average filter of a smaller width (0.05 s), we show in Fig. 7 that we can remove the variability of correlation time due to pulsatile motion and get a relatively smooth curve. From Table 2 we observe that this technique provides noise performance that is comparable to a larger width moving average filter.

Although this instrument has been designed specifically to image CBF, it can easily be adapted for other clinical measurements. For example, monitoring blood flow in burn victims can help quickly estimate tissue viability. Currently, the standard method of assessing burn depths, and hence categorizing burns, is a combination of visual inspection and patient (or witness) questionnaires. This method is empirical and often unreliable.[28] Thus, accurate assessment of tissue viability is important to evaluate and direct treatment options, estimate survival rates,

Table 2 Comparing the efficiency of the *ad hoc* ECG filter and a moving average filter. Blood flow fluctuations were filtered out using an *ad hoc* filter based on simultaneously recorded ECG waveforms. For comparison, these fluctuations were also filtered using a moving averae filter. The *ad hoc* ECG filter was found to perform better in filtering the fluctuations.

	Parenchyma %	Vessel %
Unfiltered data	12.3	13
Moving average filter (width = 0.05 s)	10.8	12.1
Ad-hoc ECG filter	4.9	5.1
ECG filter and moving average filter (width = 0.05 s)	2.5	3.2
Moving average filter (width = 0.5 s)	2.3	3.8

and calculate volume of fluid that has been lost and hence volume needed for resuscitation. Some studies have shown LSCI's potential for estimating burn depths.[29,30] LSCI can also be used during surgical recession of burnt tissue to estimate the blood flow of healthy tissue.

6 Conclusions

By incorporating an LSCI instrument to an existing surgical microscope, we have demonstrated a robust and convenient method to image CBF intraoperatively with minimal interference to the surgery. Additionally, high temporal resolutions and real-time capabilities make it a potentially useful tool for neurosurgeries. Results from the pilot study have demonstrated the feasibility of using LSCI to obtain blood flow images during neurosurgeries. Our results also demonstrate the importance of removing artifacts in the time courses due to pulsatile motion of the brain.

References

1. G. Sutherland, T. Kaibara, C. Wallace, B. Tomanek, and M. Richter, "Intraoperative assessment of aneurysm clipping using magnetic resonance angiography and diffusion-weighted imaging: technical case report," *Neurosurgery* **50**, 893–898 (2002).
2. N. Pouratian, S. Sheth, N. Martin, and A. Toga, "Shedding light on brain mapping: advances in human optical imaging," *Trends Neurosci.* **26**, 277–282 (2003).

3. A. Cannestra, S. Bookheimer, N. Pouratian, A. O'Farrell, N. Sicotte, N. Martin, D. Becker, G. Rubino, and A. Toga, "Temporal and topographical characterization of language cortices using intraoperative optical intrinsic signals," *Neuroimage* **12**, 41–54 (2000).

4. T. Schwartz, "Optical imaging of epileptiform events in visual cortex in response to patterned photic stimulation," *Cereb. Cortex.* **13**, 1287–1298 (2003).

5. E. Keller, A. Nadler, H. Alkadhi, S. Kollias, Y. Yonekawa, and P. Niederer, "Noninvasive measurement of regional cerebral blood flow and regional cerebral blood volume by near-infrared spectroscopy and indocyanine green dilution," *NeuroImage* **20**, 828–839 (2003).

6. A. Raabe, P. Nakaji, J. Beck, L. Kim, F. Hsu, J. Kamerman, V. Seifert, and R. Spetzler, "Prospective evaluation of surgical microscope-integrated intraoperative near-infrared indocyanine green videoangiography during aneurysm surgery," *J. Neurosurg.* **103**, 982–989 (2005).

7. A. Raabe, D. Van De Ville, M. Leurenegger, A. Szelenyi, E. Hattingen, R. Gerlach, V. Seifert, C. Hauger, A. Lopez, R. Leitgeb, E. Martin-Williams, and T. Lasser, "Laser doppler imaging for intraoperative human brain mapping," *NeuroImage* **44**, 1284–1289 (2009).

8. J. Briers, "Laser doppler, speckle and related techniques for blood perfusion mapping and imaging," *Physiol. Meas.* **22**, R35–R66 (2001).

9. D. Boas and A. Dunn, "Laser speckle contrast imaging in biomedical optics," *J. Biomed. Opt.* **15**, 011109 (2010).

10. A. Dunn, H. Bolay, M. Moskowitz, and D. Boas, "Dynamic imaging of cerebral blood flow using laser speckle," *J. Cereb. Blood Flow Metab.* **21**, 195–201 (2001).

11. A. Dunn, A. Devor, A. Dale, and D. Boas, "Spatial extent of oxygen metabolism and hemodynamic changes during functional activation of the rat somatosensory cortex," *NeuroImage* **27**, 279–290 (2005).

12. T. Durduran, C. Zhou, B. Edlow, G. Yu, R. Choe, M. Kim, B. Cucchiara, M. Putt, Q. Shah, S. Kasner, J. Greenberg, A. Yodh, and J. Detre, "Transcranial optical monitoring of cerebrovascular hemodynamics in acute stroke patients," *Opt. Express*, **17**, 3884–3902 (2009).

13. C. Ayata, A. Dunn, Y. Gursoy-Ozdemir, Z. Huang, D. Boas, and M. Moskowitz, "Laser speckle flowmetry for the study of cerebrovascular physiology in normal and ischemic mouse cortex," *J. Cereb. Blood Flow Metab.* **24**, 744–755 (2004a).

14. C. Ayata, H. Shin, S. Salomone, Y. Ozdemir-Gursoy, D. Boas, A. Dunn, and M. Moskowitz, "Pronounced hypoperfusion during spreading depression in mouse cortex," *J. Cereb. Blood Flow Metab.* **24**, 1172–1182 (2004b).

15. H. Shin, A. Dunn, P. Jones, D. Boas, E. Lo, M. Moskowitz, and C. Ayata, "Normobaric hyperoxia improves cerebral blood flow and oxygenation, and inhibits peri-infarct depolarizations in experimental focal ischaemia," *Brain* **130**, 1631–1642 (2007a).

16. H. Shin, P. Jones, M. Garcia-Alloza, L. Borrelli, S. Greenberg, B. Bacskai, M. Frosch, B. Hyman, M. Moskowitz, and C. Ayata, "Age-dependent cerebrovascular dysfunction in a transgenic mouse model of cerebral amyloid angiopathy," *Brain* **130**, 2310–2319 (2007b).

17. H. Shin, A. Dunn, P. Jones, D. Boas, M. Moskowitz, and C. Ayata, "Vasoconstrictive neurovascular coupling during focal ischemic depolarizations," *J. Cereb. Blood Flow Metab.* **26**, 1018–1030 (2006).

18. Y. Huang, N. Tran, P. Shumaker, K. Kelly, E. Ross, J. Nelson, and B. Choi, "Blood flow dynamics after laser therapy of port wine stain birthmarks," *Lasers Surg. Med.* **41**, 563–571 (2009).

19. N. Hecht, J. Woitzik, J. Dreier, and P. Vajkoczy, "Intraoperative monitoring of cerebral blood flow by laser speckle contrast analysis," *Neurosurg. Focus* **27**(4), E11 (2009).

20. W. Tom, A. Ponticorvo, and A. Dunn, "Efficient processing of laser speckle contrast images," *IEEE Trans. on Med. Imaging* **27**, 1728–1738 (2008).

21. *"Safe Use of Lasers,"ANSI Z136.1-2007* Laser Institute of America (2007).

22. A. Strong, E. Bezzina, P. Anderson, M. Boutelle, S. Hopwood, and A. Dunn, "Evaluation of laser speckle flowmetry for imaging cortical perfusion in experimental stroke studies: quantitation of perfusion and detection of peri-infarct depolarisations," *J. Cereb. Blood Flow Metab.* **26**, 645–653 (2006).

23. S. Yuan, A. Devor, D. Boas, and A. Dunn, "Determination of optimal exposure time for imaging of blood flow changes with laser speckle contrast imaging," *Appl. Opt.* **44**, 1823–1830 (2005).

24. R. Bandyopadhyay, A. Gittings, S. Suh, P. Dixon, and D. Durian, "Speckle-visibility spectroscopy: A tool to study time-varying dynamics," *Rev. Sci. Instrum.* **76**, 093110 (2005).

25. P. Lemieux and D. Durian, "Investigating non-Gaussian scattering processes by using n th-order intensity correlation functions," *J. Opt. Soc. Am. A* **16**, 1651–1664 (1999).

26. A. Parthasarathy, W. Tom, A. Gopal, X. Zhang, and A. Dunn, "Robust flow measurement with multi-exposure speckle imaging," *Opt. Express* **16**, 1975–1989 (2008).

27. R. H. Deckers, P. van Gelderen, M. Ries, O. Barret, J. H. Duyn, V. N. Ikonomidou, M. Fukunaga, G. H. Glover, and J. A. de Zwart, "An adaptive filter for suppression of cardiac and respiratory noise in mri time series data," *NeuroImage* **33**, 1072–1081 (2006).

28. W. Manafo, "*Treatment of Burns: Principles and Practice*", WH Green, St. Louis, MO, (1971).

29. C. Stewart, R. Frank, K. Forrester, J. Tulip, R. Lindsay, and R. Bray, "A comparison of two laser-based methods for determination of burn scar perfusion: laser Doppler versus laser speckle imaging," *Burns* **31**, 744–752 (2005).

30. A. Sadhwani, K. Schomacker, G. Tearney, and N. Nishioka, "Determination of Teflon thickness with laser speckle. I. potential for burn depth diagnosis," *Appl. Opt* **35**, 5727–5735 (1996).